

# High-Throughput Nanoindentation Mapping of a Microsegregated CoCrFeNi Multi-Principal Element Alloy (MPEA): Challenges and Limitations

Magdalena Lassinantti Gualtieri,\* Elena Colombini, Veronica Testa, Giovanni Bolelli, Roberto Giovanardi, and Paolo Veronesi

Equimolar CoCrFeNi is a popular multi-principal element alloy, generally obtained by melt-aided routes. The dendritic microstructure of as-cast alloys is cooling-rate dependent and thus may show different macromechanical behaviors. Knowledge about the nanomechanics of chemically/structurally distinct zones is important for explaining these differences and facilitating material's design through processing conditions. To this aim, high-throughput nanoindentation mapping is a potentially powerful tool. However, results are possibly biased by the indentation size effect (ISE) and plastically deformed surfaces induced by inadequate sample preparation. This work is aimed at giving some guidelines for map acquisition and sample preparation based on data from various nanoindentation techniques (i.e., high-throughput nanoindentation, continuous stiffness, and quasi-static measurements) collected on differently polished surfaces. It is shown that conventional metallographic preparation leads to a plastically deformed layer that penetrates deep into the surface (11–17  $\mu\text{m}$ ). Electropolishing is efficient in removing this layer. However, difficulties may arise due to preferential corrosion in a multiphase system wherefore polishing conditions needs optimization. Nanoindentations of adequately prepared surfaces of CoCrFeNi result in an important ISE, which affects measurements at depths lower than ca 2000 nm. This must be taken into account when performing high-throughput nanoindentation mapping of this material.

continuously being published on their various aspects.<sup>[1–3]</sup> High entropy alloys (HEAs), also encompassed in this group of materials, have the more restrictive definition of being entropy-stabilized single-phase solid solutions (SS) composed of five or more elements with concentrations in the range 5–35 at%.<sup>[1–3]</sup> A big portion of the published research specifically deals with alloys fitting the HEA definition and in particular face-centered cubic (fcc) SS structures being composed of 3d transition metals. The so-called Cantor alloy (i.e., equimolar FeNiCrCoMn) and its derivatives are particularly in focus.<sup>[3]</sup> Among all possible modifications of the Cantor alloy, equimolar CoCrFeNi has received particular attention.<sup>[3]</sup> Not only does this alloy possess interesting mechanical properties<sup>[4]</sup> and high resistance to corrosion,<sup>[5]</sup> but also its phase stability over a wide range of temperatures renders it an interesting matrix for complex microstructures containing precipitation strengthening phases<sup>[6–9]</sup> or grain growth inhibitors such as oxides and carbides.<sup>[10]</sup>

The as-cast CoCrFeNi alloy is known to crystallize in an fcc structure, sometimes reported to have a certain degree of microsegregation with Cr accumulated in the grain boundaries.<sup>[11,12]</sup> Accelerated cooling from the melted state may even lead to the crystallization of a Cr-rich bcc phase in the interdendritic region that leads to an overall increase in microhardness.<sup>[11]</sup>


The cooling-rate dependence of microstructure and mechanical properties of as-cast HEAs has been investigated in more detail by others.<sup>[13,14]</sup> Knowledge about the nanomechanics of distinct zones, differing in structure and/or chemical composition, is advantageous for the interpretation of macroscopic mechanical properties and the understanding of processing–microstructure–macromechanical relations. To this aim, nanoindentation is a highly valuable tool. However, correct positioning of the indenter in specific zones with small length scales is challenging in traditional nanoindentation. A promising alternative that potentially resolves this problem is offered by high-throughput nanoindentation techniques.<sup>[15,16]</sup> The high measurement speed (as many as 6 indentations/s<sup>[16]</sup>)

## 1. Introduction

The research interest in multi-principal element alloys (MPEAs) or complex concentrated alloys (CCAs) is continuously growing as witnessed by the large number of review articles that are

M. Lassinantti Gualtieri, E. Colombini, V. Testa, G. Bolelli, R. Giovanardi, P. Veronesi

Department of Engineering “Enzo Ferrari”  
University of Modena and Reggio Emilia  
Via P. Vivarelli 10/1, 41125 Modena, Italy  
E-mail: magdalena.gualtieri@unimore.it

 The ORCID identification number(s) for the author(s) of this article can be found under <https://doi.org/10.1002/adem.202300110>.

© 2023 The Authors. Advanced Engineering Materials published by Wiley-VCH GmbH. This is an open access article under the terms of the Creative Commons Attribution License, which permits use, distribution and reproduction in any medium, provided the original work is properly cited.

DOI: 10.1002/adem.202300110

enables the collection of huge datasets, covering large areas in a short period of time, which allows to statistically separate the mechanical properties of different phases/zones. Generally, this includes modeling of frequency distribution curves of the properties with Gaussian functions. The 2D maps of the mechanical properties (i.e., hardness and elastic modulus) are generally superimposed with other microstructural information collected by, e.g., scanning electron microscopy–energy dispersive X-ray spectroscopy (SEM–EDS) to obtain a comprehensive picture of the relationships between microstructural features and mechanical properties. These types of multidimensional datasets are increasingly being used for the characterization of microstructurally heterogeneous MPEAs.<sup>[17–23]</sup> For example, Coury et al. recently performed high-throughput nanoindentations on a compositionally-graded sample in the CoCrFeNiMn HEA system<sup>[20]</sup> and found a good correlation between experimental results and predicted solid solution strengthening represented by atomic size mismatch. The authors highlighted the potential of high-throughput nanoindentation mapping of samples with controlled chemical gradients for fast screening of a vast multicomponent space.<sup>[20]</sup>

High-throughput nanoindentation mapping requires careful consideration of various factors that may affect the results.<sup>[15,16]</sup> The spacing between indents must be carefully chosen to avoid overlap of pile-ups and plastic zones from adjacent indentations.<sup>[15,16]</sup> Hence, higher resolution is necessarily accomplished by employing relatively low values of the maximum penetration depth/maximum load. This general requirement opens up some problems related to the measurement itself, for example, the indentation size effect (ISE)<sup>[24–28]</sup> and inadequately prepared surfaces,<sup>[29–32]</sup> both of which are valid concerns for nanoindentation in general but in particular for high-resolution mapping where the penetration depth generally is low.<sup>[15]</sup>

This work reports, for the first time, high-throughput nanoindentation mapping of a solidification structure of the popular CoCrFeNi alloy. In addition, continuous stiffness measurements (CSM) and quasi-static nanoindentations as well as microindentations were also performed. The sample, extensively investigated in a previous work,<sup>[12]</sup> is structurally homogeneous (fcc) but exhibits a typical dendritic–interdendritic microstructure with segregation of Cr in the interdendritic region. As solid solution strengthening in HEAs can lead to remarkable increases in hardness and is strongly dependent on the chemical composition,<sup>[20,21,33]</sup> it was hypothesized that the observed microsegregation would be reflected in high-throughput nanohardness maps and that statistical elaboration of the measurement output would be useful in determining the individual mechanical properties of the specific phases. It will be shown that the accuracy of this type of measurement is highly influenced by the metallographic preparation procedure (chemical–mechanical polishing, electropolishing) and that the ISE of this alloy is important up to depths largely exceeding those normally used for high-resolution indentation mapping. The results thus give some valuable inputs for correct sample preparation and execution of high-throughput nanoindentation mapping of this common MPEA.

## 2. Results and Discussions

### 2.1. High-Speed Nanoindentation on a Chemically–Mechanically Polished Sample

The equimolar bulk FeNiCrCo alloy investigated in this work was synthesized by melting of prealloyed powders followed by natural cooling (see ref. [12] for further details). The resulting sample exhibits a dendritic–interdendritic microstructure with the interdendritic region being enriched in Cr and depleted in Co and Fe.<sup>[12]</sup> This microsegregated fcc solid solution is typical of an as-cast alloy with a low degree of undercooling.<sup>[11]</sup> According to X-ray powder diffraction (XRPD) data published in the previous work,<sup>[12]</sup> the alloy is a pure fcc solid solution. Different cell constants of the chemically different regions are expected due to marginally different atomic radii of the constituting elements.<sup>[34,35]</sup> However, the low resolution of in-house instruments does not allow to quantify the slightly different fcc structures.<sup>[35]</sup> A promising technique to distinguish the different structures and to determine their distinct mechanical properties is high-throughput nanoindentation mapping with statistical elaboration of large data sets.<sup>[20]</sup> In fact, solid solution-strengthening effects in MPEAs are important and strongly dependent on the composition.<sup>[20,21,33]</sup> Hence, a spatial variation of the mechanical properties in the microsegregated bulk can be hypothesized. According to SEM-EDS analyses, the interdendritic Cr-rich area is about 25–30  $\mu\text{m}$  large, see Figure S1, Supporting Information. Therefore, nanoindentation tests with a maximum penetration depth of about 300 nm (Section 4) should have sufficient spatial resolution to explore the mechanical properties of chemically distinct regions.<sup>[20,36]</sup>

**Figure 1** shows the surface map of the Vickers hardness ( $HV_{IT}$ ), calculated from the indentation hardness ( $H$ ), along with the EDS elemental map of Cr recorded from a limited region of the area subjected to hardness mapping (indicated by a rectangle). Large variations in surface hardness are observed, but these variations do not appear to be connected to the microsegregated microstructure (Figure 1). The average Vickers hardness ( $HV_{IT}$ ) and reduced plane-strain elastic modulus ( $E^*$ ) are  $549 \pm 42$  and  $247 \pm 15$  GPa, respectively. **Figure 2** shows the relative frequency

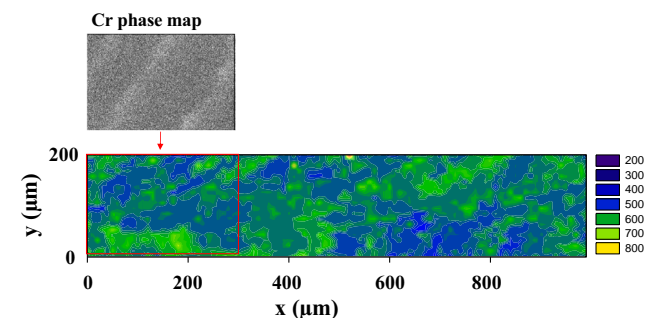


**Figure 1.** Surface map in 2D of the Vickers hardness ( $HV_{IT}$ ) calculated from the indentation hardness ( $H$ ) of the CoCrFeNi bulk subjected to chemical–mechanical polishing. The EDS map of Cr collected from a limited area of the indentation map (indicated by a red rectangle) is also shown.

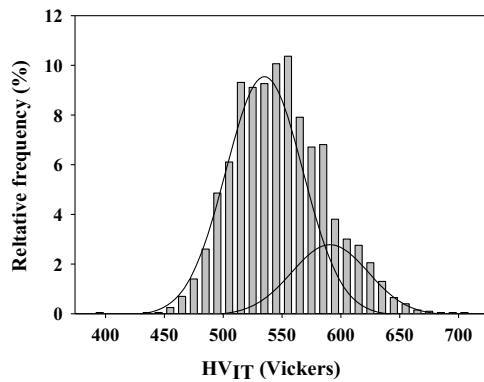


**Figure 2.** Relative frequency as a function of Vickers hardness ( $HV_{IT}$ ) calculated from the indentation hardness ( $H$ ). The distribution appears to be bimodal. The continuous lines represent Gaussian functions fitted to the experimental data using the least squares method.

as a function of Vickers hardness. An asymmetric distribution is observed, which could indicate a predominant distribution function with a lower mean hardness and another one with a higher mean hardness but in a lower volume fraction. Indeed, a good fit of the experimental data was obtained with the sum of two overlapping Gaussian functions (see Figure 2). The Vickers hardness ( $HV_{IT}$ ) of the first and second peaks were determined to be  $535 \pm 4$  and  $591 \pm 10$ , respectively. The corresponding peak areas were  $785 \pm 97$  and  $232 \pm 7$  ( $HV_{IT} \times$  relative frequency).

Thus, high-throughput nanoindentation mapping of the chemically–mechanically polished sample did not reproduce the segregated microstructure observed from EDS mapping, see Figure 1. Instead, a somewhat banded appearance of softer and harder areas is observed which may be quantified by statistical elaboration using both Gaussian fitting of the relative frequency distributions (Figure 2). Considering that microsegregation during solidification is the only apparent microstructural feature observed in the sample, it can be assumed that the high-throughput nanoindentation hardness map does not reflect the sample’s true microstructure. The bimodal frequency distribution of hardness, with peaks at ca 535 and 591  $HV_{IT}$  (see Figure 2), reveals values considerably higher than previously reported values from bulk CoCrFeNi determined under similar conditions.<sup>[33,37]</sup> Yang et al. performed CSM on various Ni-based alloys including CoCrFeNi for which an important indentation size effect (ISE) was observed that caused a decrease in nanohardness from 3.75 to 1.95 GPa when the penetration depth increased from 200 nm to 2000 nm.<sup>[33]</sup> The bulk hardness ( $H_0$ ), determined from Nix–Gao modeling,<sup>[24]</sup> was ca 1.6 GPa.<sup>[33]</sup> Zhang et al. performed nanoindentations on CoCrFeNi $_x$  HEAs ( $x = 0–0.3$ ) using a maximum load of 5 mN, resulting in penetration depths  $<220$  nm.<sup>[37]</sup> The authors reported a nanohardness of 2.9 GPa for the CoCrFeNi base alloy. They did not evaluate the influence of ISE on the samples under study but acknowledged that the measured values could indeed be affected by this phenomenon.

A possible explanation of the high nanohardness values shown in Figure 2, too high to be explained simply by ISE considering the work by others,<sup>[33,37]</sup> resides in different degrees of work hardening at different locations on the surface of the

chemically–mechanically polished sample. The bands with higher hardness observed in Figure 1 might be reminiscent of grooves produced by grinding with SiC papers, rather than of differences in solid solution hardening between the dendritic and interdendritic regions. While the grooves were smoothed down during chemical–mechanical polishing to yield a mirror-polished surface, the subsurface work hardening associated with those grooves was possibly preserved in the sample. Chemical–mechanical polishing was likely unable to remove all of the work-hardened region, and/or it might have introduced some further work hardening. Thus, the density of structural defects produced by the mechanical action is apparently not homogeneous and could in fact reflect differences not only in the distribution of the stress imposed by grinding/polishing but also in the mechanical response of distinct grains due to, e.g., crystallographic orientation.

Problems related to surface preparation for nanoindentation have frequently been addressed for various materials over the last decades.<sup>[29–32]</sup> Nevertheless, this topic continues to deserve attention as many recent studies do not stress this aspect, and in many cases, the sample preparation procedures are not even reported. Work hardening during metallographic preparation is most apparent with soft materials. Wang et al. investigated the effect of surface finish (different mechanical polishing procedures as well as electropolishing) on load-controlled nanoindentation experiments on single-crystal Mo, aiming to determine the transition from elastic to plastic deformation through pop-in loads.<sup>[29]</sup> The authors concluded that both mechanical (0.05  $\mu\text{m}$  alumina) as well as chemical–mechanical (0.02  $\mu\text{m}$  colloidal silica) polishing cause enough surface damage to prevent the occurrence of pop-ins whereas the response from electropolished surfaces indicates a defect-free structure.<sup>[29]</sup> Pathak et al. investigated the effect of surface finish (electropolishing and mechanical polishing using 1  $\mu\text{m}$  diamond paste in the final step) on the indentation curves obtained by spherical nanoindentation.<sup>[30]</sup> Both annealed aluminum and tungsten were investigated as these materials show large differences in elastic modulus and yield strength. The authors found an important effect of surface finishes on the indentation curves for both materials, showing smaller peak loads to attain the same maximum displacements for electropolished samples.<sup>[30]</sup> The same qualitative differences were observed by Bahr et al. between the indentation curves obtained from mechanically polished and electropolished single-crystal tungsten.<sup>[31]</sup> Considering the numerous studies cited above, it appears that electropolishing is an efficient method to remove subsurface damage caused by mechanical polishing. Hence, step-wise electropolishing was performed followed by quasi-static and CSM as well as microindentation with the aim of investigating subsurface damage caused by conventional metallographic preparation. Profilometry measurements of the polished surfaces were performed to determine the thickness of the removed layers following each step.

## 2.2. Profilometry Across the Interface Between Differently Polished Regions

**Figure 3** shows 3D topographical maps acquired across the interface between the mechanically–chemically polished areas

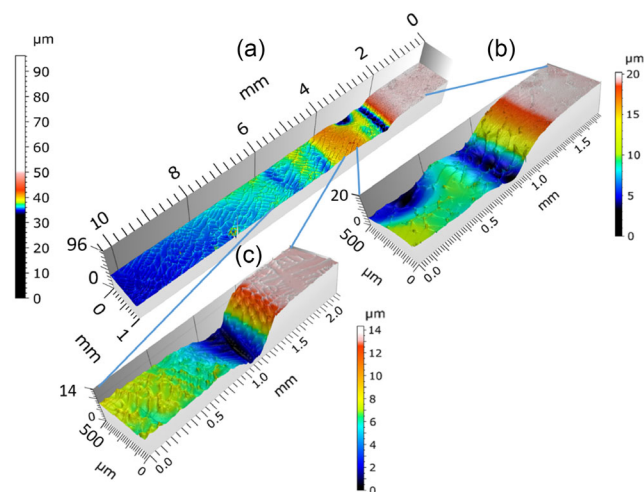


**Figure 3.** 3D topographical maps of the electropolished sample. The non-treated area and the areas subjected to two and three voltage cycles are shown in (a). The interfaces between the differently treated zones, as indicated in (a), are better viewed in (b) and (c). See text for details.

and the electropolished (EP) ones. As described in the Experimental Section, two separate EP experiments were conducted (two voltage cycles in the first experiment and one additional voltage cycle in the second one) with CSM nanoindentation measurements in between. The second experiment was executed on a slightly smaller area with respect to the first one, thus enabling to observe the layer removed in the two electropolishing sessions. The first thing to notice from the figure is that the EP process leaves a textured surface due to preferential etching of the dendritic region, leaving the interdendritic network in relief. This was indeed also observed from SEM images of indented areas shown in Figure S2, Supporting Information.

The extracted step height between the chemically–mechanically polished region and the region exposed to two voltage cycles (first experiment) was  $\approx 11 \mu\text{m}$  (Figure 3b) whereas the layer removed in the subsequent single voltage cycle was  $\approx 6 \mu\text{m}$  (Figure 3c). The overall etching rate is thus  $1 \mu\text{m min}^{-1}$  (considering that one single EP cycle, from 0 V to 9 V and from 9 V to 0 V, lasts 6 min). Guo et al. found a material removal rate of  $5 \mu\text{m min}^{-1}$  during electropolishing of CoCrFeMnNi using similar conditions (i.e., same chemical solution, but applying a constant potential of 12.5 V that is higher than the potential used for our work).<sup>[38]</sup>

### 2.3. Quasi-Static Indentations on and Continuous Stiffness Measurements on Differently Polished Samples

CSM offers the possibility to measure the contact stiffness continuously along the loading curve. Thus, it is a valuable tool for evaluating in-depth changes in the microstructure and mechanical properties of multilayer materials.<sup>[39]</sup> Hence, it was considered a suitable technique to evaluate possible subsurface damage caused by metallographic sample preparation. In addition, the technique also allows to collect a large number of hardness profiles in a limited amount of time.

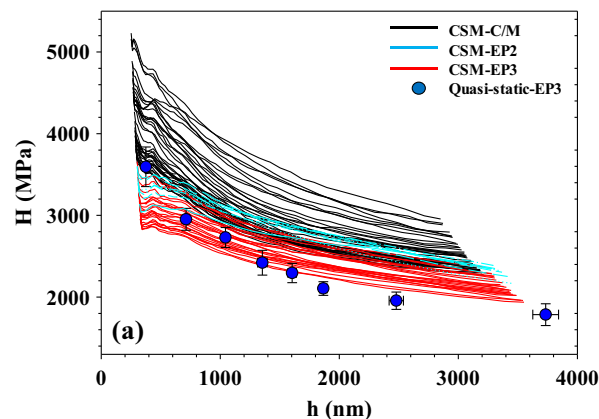


**Figure 4.** Results from CSM. Nanoindentation hardness (H) as a function of penetration depth (h) following: chemical–mechanical (C/M) polishing (black lines); electropolishing, two cycles (EP2, light blue lines); electropolishing, three cycles (EP3, red lines). For comparison, data obtained from quasi-static indentations are also shown (blue circles).

**Figure 4** shows the hardness as a function of penetration depth, calculated from CSM, for the chemically–mechanically polished CoCrFeNi bulk before (black) and after each of the two electropolishing experiments (EP2 light blue, EP3 red). For comparison, data collected from quasi-static nanoindentations following three electropolishing cycles are also shown (EP3, blue circles). The quasi-static indentation curves from which the data in Figure 4 were derived are shown in the supporting information (Figure S3, Supporting Information). Only indentations performed in the dendritic regions were considered (identified from SEM images, see Figure S2a, Supporting Information) as the interdendritic zones were in relief due to a slower etching.

As can be observed from the figure, the hardness is successively shifted to lower values going from the chemically–mechanically polished surface to the electropolished ones using two voltage cycles (EP2) and three voltage cycles (EP3). The CSM data for the electropolished sample (EP3) are close to, though not exactly coincident with, the results from quasi-static indentations performed on the same surface (Figure 4). Differences between hardness profiles obtained by CSM and quasi-static measurements have frequently been addressed in the literature and explained by the occurrence of dynamic unloading that causes important measurement errors even at low amplitude if the contact stiffness is high (i.e., high modulus-to-hardness ratio).<sup>[40,41]</sup> In addition, noisy and unreliable data are produced at very shallow indentations due to the detachment of the indenter from the surface.<sup>[41]</sup> These problems can in part be mitigated by reducing the amplitude of the displacement oscillation.<sup>[40,41]</sup> For example, Ruiz-Moreno and Hälner recently investigated the ISE on ferritic/martensitic steels using both quasi-static and force-controlled CSM mode, the latter including different amplitudes (5–20% of  $F_{\text{max}} = 100 \text{ mN}$ ) and frequencies (10–100 Hz) of the superimposed sinusoidal oscillation.<sup>[40]</sup> The authors found that the hardness values in the nano-regime were shifted to lower values when the oscillation amplitude increased.<sup>[40]</sup> The closest agreement between quasi-static measurements and CSM was



observed at the lowest applied amplitude,<sup>[40]</sup> in accordance with previous work.<sup>[41]</sup> The relatively large oscillation amplitude used here (50 mN) likely caused the mentioned deviations at low penetration depth with respect to the quasi-static measurements (see Figure 4). Despite possible aberrations of the indentation response to the applied oscillating force, CSM data collected from the two differently finished surfaces can be compared and their different responses assigned to the characteristics of the samples. The curves depicted in Figure 4 show an exponential decay with higher decay rates for the chemically–mechanically polished sample (see Figure S4, Supporting Information, for fitting curves). The higher decay rate in the chemically–mechanically polished sample is mainly assigned to a gradual decrease in sub-surface damage whereas the residual hardness gradient in the sample electropolished using three voltage cycles is assigned mainly to the ISE. ISE is a well-known and deeply investigated phenomenon occurring in nanoindentation experiments and most commonly manifested as an increased recorded hardness at lower penetration depth of the indenter. A still popular and simple mechanistic description of the size effect based on the Taylor dislocation model was developed by Nix and Gao<sup>[24]</sup>

$$\frac{H}{H_0} = \sqrt{1 + \frac{h^*}{h}} \quad (1)$$

where  $H$  is the experimentally determined nanoindentation hardness,  $H_0$  is the bulk hardness,  $h$  is the penetration depth of the indenter, and  $h^*$  is the characteristic depth (threshold under which ISE is important). A plot of  $H^2$  as a function of  $1/h$  should be linear enabling the determination of both  $H_0$  and  $h^*$  from the intercept and slope (i.e.,  $H_0$  is the square root of the intercept and  $h^*$  is calculated from the slope =  $H_0^2 \times h^*$ ). The core of this model assumes that the ISE is related to geometrically necessary dislocations (GNDs) in the plastically deformed region formed under the tip of the indenter and that the density of these dislocations is inversely proportional to the penetration depth. Numerous studies have however reported deviation from the linearity of the Nix–Gao plot at low penetration depths and many modifications of the original model of Nix and Gao have been suggested to account for the breakdown of the scaling regime.<sup>[42]</sup> In recent work, Haušild critically compared existing breakdown models and proposed a new correction of the Nix–Gao model that accurately predicted the hardness profiles for a wide variety of materials (including a refractory HEA) showing dislocation-mediated plastic deformation

$$\frac{H}{H_0} = \sqrt{1 + \frac{h^*}{h} \left(1 - e^{-\frac{h}{h_1}}\right)^n} \quad (2)$$

where  $h_1$  is a parameter and  $n$  is an exponent (shape parameter).<sup>[42]</sup>

Figure 5 shows the results from modeling of the quasi-static nanoindentation data with Nix–Gao<sup>[24]</sup> (Equation (1)) and the modified Nix–Gao equation suggested by Haušild<sup>[42]</sup> (Equation (2)). For comparison, the CSM data for the same sample (mean curve) is also shown together with CSM data collected by others for the same alloy (i.e., (100) surface of a single-crystal CoCrFeNi).<sup>[33]</sup> First of all, the curve calculated from the quasi-static data appears to deviate from linearity in the nanorange,

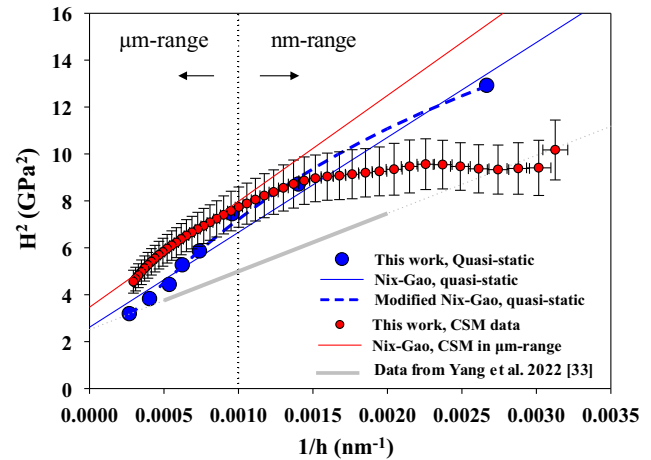


**Figure 5.** Results from data modeling of quasi-static nanoindentation data (electropolished with 3 voltage cycles, EP3) with Nix–Gao<sup>[24]</sup> (Equation (1)) and the modified Nix–Gao<sup>[42]</sup> (Equation (2)). The experimental data (blue circles) rather clearly show a breakpoint of the linear trend in the nanorange. For comparison, the mean curve of the CSM measurements for the same sample is shown together with the fit with the linear Nix–Gao model. CMS data for a similar alloy (single-crystal CoCrFeNi) reported by others are also shown.

even though some uncertainty is given by the small number of data points in this region. This breakdown of the scaling regime is effectively fitted with the modified model (Equation (2)), giving the following fitting parameters:  $H_0 = 1.15$  GPa,  $h^* = 4866$  nm,  $h_1 = 106$  nm, and  $n = 0.80$ . Instead, the linear Nix–Gao model gives a  $H_0$  of 1.617 GPa and a characteristic depth ( $h^*$ ) of 1548 nm. By comparing these numbers, it is evident that not considering the breakpoint in the classical Nix–Gao plot may lead to a drastic overestimation of the bulk hardness ( $H_0$ ). The difference between data collected by quasi-static and CSM methodology is evident, as already observed in Figure 4. In this case, the important deviation from linearity, particularly in the nanorange, is most likely caused by the measurement methodology itself rather than a true breakdown of the Nix–Gao model due to materials characteristics. If only data points in the micrometer regime are considered, the linear Nix–Gao model of the mean curve shown in Figure 5 gives a  $H_0$  of 1.86 GPa and a characteristic depth ( $h^*$ ) of 1302 nm.

It is interesting to observe that modeling of CSM data collected by others for a similar alloy (i.e., (100) surface of a single crystal of CoCrFeNi,<sup>[33]</sup> see Figure 5) in the range 500–2000 nm was highly linear and yielded a bulk hardness ( $H_0$ ) before pile-up correction of 1.60 GPa.

Based on the data presented in Figure 4 and 5, it can be stated that an apparent size effect is observed in the chemical–mechanically polished sample which is mainly attributed to surface work hardening. It was found necessary to remove an 11–17  $\mu\text{m}$  thick layer from the chemically–mechanically polished sample to measure the “true” properties of the dendritic areas. In fact, the nanohardness measured after the first series of two electropolishing steps was still marginally higher than the result after the third electropolishing step (Figure 4), which means that the work-hardened depth was slightly higher than 11  $\mu\text{m}$

(the depth removed during the first two EP cycles) but lower than 17  $\mu\text{m}$  (the total depth removed after the third cycle). Even if this damaged layer is removed by electropolishing, a rather steep change in hardness with penetration depth is still observed down to about 2000 nm (see Figure 4), a phenomenon attributed to the ISE. Yang et al. recently found that the ISE of different solid solutions of 3d transition metal alloys may vary depending on the chemical composition.<sup>[33]</sup> This result is highly interesting as it implies that ISE can cause contrast in high-throughput hardness maps which possibly is not reflecting the bulk hardness contrast. This should be considered when interpreting data collected from these materials at shallow depths.

## 2.4. Microhardness on Differently Polished Samples

Vickers indentations using a force of 1000 mN were performed following chemical–mechanical polishing as well as after additional electropolishing using three voltage cycles (EP3). The Vickers hardness ( $HV_{0.1}$ ) calculated according to Equation (3) was  $247 \pm 12 HV_{0.1}$  and  $160 \pm 7 HV_{0.1}$  before and after EP3, respectively. The corresponding penetration depths, which were estimated from the indentation diagonal ( $d$ ) knowing that, for the Vickers indenter geometry, the penetration depth is approximately  $1/7$  of  $d$ ,<sup>[43]</sup> were  $4.0 \pm 0.1$  and  $4.9 \pm 1 \mu\text{m}$ . This means that, on the one hand, the thickness of the work-hardened layer on the chemically–mechanically polished sample, which was estimated to be in the range 11–17  $\mu\text{m}$ , is consistently higher than the microindentation depth of 4  $\mu\text{m}$ . On the other hand, microindentation experiments performed on the electropolished (EP3) sample returned hardness values that were very close to the “bulk hardness,  $H_0$ ” from the Nix–Gao modeling of nanoindentation data. In fact, the microindentation depths between 4 and 5  $\mu\text{m}$  are comparable to the above-mentioned characteristic depth  $h^* = 4866 \text{ nm}$  from the modified Nix–Gao model applied to quasi-static nanoindentations, i.e., the microindentations fall in the range where ISE is not much perceivable any more. Microindentation tests thus provided additional confirmation to the results of nanoindentation analysis.

## 3. Conclusion

In this work, high-throughput nanoindentation mapping, as well as quasi-static and dynamic nanoindentation measurements, were performed on a microsegregated solidification structure of a crystallographically homogeneous CoCrFeNi MPEA. The following main conclusions were made: 1) Surface preparation for nanoindentation of CoCrFeNi must include a final polishing step, such as electropolishing, that removes subsurface damage caused by conventional metallographic preparation. Otherwise, falsified measurement results may be obtained. 2) The work-hardened layer formed by standard metallographic polishing, which needs to be removed by the final polishing (e.g., electropolishing) stage, was estimated to be 11–17  $\mu\text{m}$  thick. 3) Although electropolishing is effective in removing subsurface damage caused by conventional metallographic preparation, difficulties may arise due to differential dissolution rates in a multiphase system. This is particularly problematic for high-throughput nanoindentation mapping aimed at revealing the

mechanical properties of each constituting phase. Indeed, surface textures due to such differential dissolution might make it impractical or impossible to indent one or more phases. Hence, work is needed to optimize the electropolishing process or explore other potential solutions such as vibro-polishing,<sup>[15,30]</sup> in both cases considering the thickness of the plastically deformed layer that needs to be removed. 4) Nanoindentation of adequately prepared CoCrFeNi surfaces results in an important ISE which affects measurements with penetration depths lower than ca 2000 nm. This should be taken into account when planning high-throughput nanoindentation mapping of this alloy. 5) The ISE is better captured by quasi-static indentations than by dynamic indentations using the continuous stiffness measurement, where a series of factors contribute to introducing artifacts that cause the measured hardness-versus-depth response to deviate from the actual one, especially in the nanometer penetration range.

## 4. Experimental Section

**Sample Preparation:** The equimolar CoCrFeNi bulk alloy investigated in this work was obtained by melting a prealloyed powder followed by solidification during natural cooling in an electric furnace with Ar atmosphere, as described in a recent work.<sup>[12]</sup> Although structurally homogeneous (fcc), the typical dendritic–interdendritic microstructure of the bulk shows segregation of Cr and Co in the interdendritic region.<sup>[12]</sup>

The bulk alloy was cut using a low-speed cutting machine (Micromet, Remet, Bologna, Italy) equipped with an abrasive disk made of alumina embedded in resin (Struers). An aqueous cutting fluid containing a lubricant was used during the operation. Embedded samples (hot-mounted in phenol resin) were subjected to metallographic preparation including sequential grinding up to a mesh size of P2000 (SiC abrasive papers) followed by polishing using diamond slurries (3  $\mu\text{m}$  and 1  $\mu\text{m}$ ). A final mirror finish was accomplished by using a colloidal silica dispersion ( $\approx 60 \text{ nm}$ ) applied on a short-napped cloth.

Electropolishing (EP) was performed to remove any plastically deformed material that could have been induced by mechanical grinding/polishing. EP was conducted in a solution of sulfuric acid (20% v/v) in methyl alcohol. Experiments were performed at room temperature using a copper plate as counter-electrode and a VersaSTAT 3 potentiostat/galvanostat as voltage source. An EP cycle included a voltage ramp from 0 V to 9.0 V and a backward scan from 9.0 V to 0 V, both with a scan rate of  $0.05 \text{ V s}^{-1}$ . Similar conditions were used by Guo et al. for electropolishing of equimolar CoCrFeMnNi alloys obtained by 3D printing technology.<sup>[38]</sup> At first, the sample was subjected to two consecutive polishing cycles on which CSM were performed. A third electropolishing cycle was successively applied but this time covering a slightly smaller area of the sample with respect to the first two cycles. In this way, the amount of material removed in the two separate electropolishing experiments could be evaluated by 3D topographical maps as will be described below. The sample surface exposed to a total of two and three electropolishing cycles will from now on be called EP2 and EP3, respectively.

**Profilometry:** To check the actual amount of material removed by electropolishing, 3D topographical maps were acquired across the interface between the chemically–mechanically polished area and the electropolished ones using a noncontact profilometer operated in structured-light mode (ConfoSurf, ConfoVis GmbH, Jena, Germany). By stitching together several maps acquired at either  $5\times$  or  $10\times$  magnification, stripes of approximately 1 mm or 500  $\mu\text{m}$  width (respectively), with a length of some millimeters in both cases, were obtained and processed with the MountainsMap software (v. 3.2) to extract the step height between the differently treated surfaces (i.e., chemically–mechanically polished, electropolished in two cycles EP2, electropolished in three cycles, EP3).

**Hardness Measurements: Nanoindentations:** Instrumented nanoindentation tests were executed using a depth-sensing nanoindenter (NHT<sup>3</sup>, Anton Paar TriTec, Corcelles - CH) accessorized with a diamond Berkovich tip which was calibrated and verified using a standard fused silica sample (10 indentations). At 80 mN, the applied load recommended by the manufacturer for tip calibration, the reduced plane-strain Young's modulus ( $E^*$ ) was determined to be  $74.0 \pm 0.9$  GPa. This value is in good accordance with the one certified by the manufacturer (i.e., 75.3 GPa).

The maximum load allowed by the instrument is 500 mN, which restricts the maximum penetration depths achievable by the indenter ( $<4 \mu\text{m}$  for the CoCrFeNi MPEA investigated here). The load-penetration depth data were analyzed by the Oliver-Pharr method.<sup>[44]</sup> The instrument was used to perform three different procedures: 1) High-speed mapping after chemical-mechanical polishing aimed at exploring possible differences in mechanical properties between the dendritic and interdendritic zones in the solidification structure (see previous work for sample details<sup>[12]</sup>). This experiment was not performed on electropolished samples due to the textured surface which resulted from preferential etching of the dendritic region. 2) CSM for depth profiling of mechanical properties using the sinus mode during loading. The sample was evaluated following chemical-mechanical polishing and after each of the two electropolishing experiments (EP2 and EP3). Only data collected from the dendritic regions were considered for electropolished samples as the curvatures of the interdendritic region, in relief due to slower etching rate, were considered far from ideal. In fact, the breadth of these elevated zones was approximately the same as the side of the triangular imprint of the Berkovich tip at a maximum load of 500 mN ( $\approx 28 \mu\text{m}$ ). Hence, even an imprint perfectly centered in the interdendritic area would inevitably be affected by the local convexity and the lateral slopes down to the dendritic areas. With the aid of secondary electron SEM images of the indented area, the position of each singular imprint could be identified (interdendritic, dendritic, or interface between the two) on the basis of surface texture generated by differential etching rate during electropolishing, see Figure S2a, Supporting Information. 3) Conventional quasi-static indentations at various loads on the sample subjected to three electropolishing cycles (EP3). Again, only data collected in the dendritic region were identified by secondary electron SEM images of the indented area (see Figure S2b, Supporting Information).

**Hardness Measurements: Nanoindentations: High-Speed Mapping:** An array of  $20 \times 100$  imprints ( $10 \mu\text{m}$  apart) was made so as to cover a rectangular area of size  $1000 \times 900 \mu\text{m}^2$ . The number of imprints and their areal spread were chosen to include the chemical variations observed in the solidification structure of the investigated bulk MPEA (dendritic-interdendritic solidification structure on an equimolar CoCrFeNi described in detail in previous work<sup>[12]</sup>). A maximum load of 10 mN was chosen, which corresponds to a penetration depth of about 300 nm. The distance of  $10 \mu\text{m}$  between imprints is about three times higher than the minimum indent spacing recommended, for example, by Sudharshan Phani and Oliver.<sup>[45]</sup> A loading/unloading rate of  $600 \text{ mN min}^{-1}$  was applied with a pause of 1 s. A frequency histogram of the Vickers hardness ( $HV_{IT}$ , calculated from the indentation hardness  $H$ ) was fitted with the sum of two Gaussian functions using the method of least squares. This approach is common to separate different populations of phases with distinct properties.<sup>[46]</sup>

**Hardness Measurements: Nanoindentations: Continuous Stiffness Measurements:** The so-called sinus mode in the Anton Paar instrument was applied to obtain the mechanical properties as a function of penetration depth in one single indentation. A strain-controlled CSM mode (constant strain rate of  $0.1 \text{ s}^{-1}$ ) was performed, which consists of a sinusoidal oscillation superimposed onto an exponentially increasing base load (maximum load of 500 mN). The frequency and amplitude of the oscillation were 5 Hz and 50 mN, respectively. These harmonic parameters were recommended by the manufacturer for the applied maximum load of 500 mN. About 50–60 indentations, distanced  $100 \mu\text{m}$  from each other, were accomplished for each sample. For the reasons discussed above, indentations in the dendritic area were selected through secondary electron SEM images and used for further elaboration (Figure S2a, Supporting Information).

**Hardness Measurements: Nanoindentations: Quasi-Static Indentations:** The applied test conditions were as follows: loading/unloading time of 30 s up to maximum loads of 10, 30, 60, 90, 120, 250, and 500 mN (instrumental maximum load). The arrays of 40 indentations for each load were accomplished and imprints in the dendritic regions were identified by SEM analyses (Figure S2b, Supporting Information) and used as the basis for discussions.

**Hardness Measurements: Microindentations:** Depth-sensing Vickers microindentations were performed using a Micro-Combi Tester (CSM Instruments). The measurements were performed on a surface subjected to chemical-mechanical polishing and on an electropolished surface (three voltage cycles, EP3). Only imprints in the dendritic regions were considered. The chemically-mechanically polished samples were identified by superimposing SEM images of the indented zone with EDS phase maps of Cr (enriched in the interdendritic area) as done in a previous work.<sup>[12]</sup> For the electropolished sample, positioning of the indenter in the dendritic region was easily accomplished with the aid of the optical microscope. A maximum load of 1000 mN was applied, using a dwell time of 15 s. A total of about 20 indentations were performed. The Vickers hardness (HV) was calculated from the indenter load ( $L$ , kgf) and the diagonals ( $d$ , mm) of the imprints according to the following well-known equation<sup>[43]</sup>

$$HV = 1.8544 \frac{L}{d^2} \quad (3)$$

## Supporting Information

Supporting Information is available from the Wiley Online Library or from the author.

## Conflict of Interest

The authors declare no conflict of interest.

## Data Availability Statement

The data that support the findings of this study are available from the corresponding author upon reasonable request.

## Keywords

high entropy alloy, indentation size effect, multi-principal element alloy, nanoindentation, plastic deformation

Received: January 24, 2023

Revised: May 31, 2023

Published online:

- [1] D. B. Miracle, O. N. Senkov, *Acta Mater.* **2017**, *122*, 448.
- [2] E. P. George, *Nat. Rev. Mater.* **2019**, *4*, 515.
- [3] F. D. C. Filho, R. O. Ritchie, M. A. Meyers, S. N. Monteiro, *J. Mater. Res. Technol.* **2022**, *17*, 1868.
- [4] Z. Wu, H. Bei, G. M. Pharr, E. P. George, *Acta Mater.* **2014**, *81*, 428.
- [5] C. Wang, J. Yu, Y. Yu, Y. Zhao, Y. Zhang, X. Han, *J. Mater. Res. Technol.* **2020**, *9*, 8482.
- [6] F. Zheng, G. Zhang, X. Chen, X. Yang, Z. Yang, Y. Li, J. Li, *Mater. Sci. Eng., A* **2020**, *774*, 138940.
- [7] S. Muskeri, B. Gwalani, S. Jha, A. Yu, P. A. Jannotti, R. S. Haridas, B. E. Schuster, J. T. Lloyd, R. S. Mishra, S. Mukherjee, *Sci. Rep.* **2021**, *11*, 22715.

- [8] W. H. Liu, J. Y. He, H. L. Huang, H. Wang, Z. P. Lu, C. T. Liu, *Intermetallics* **2015**, 60, 1.
- [9] W. H. Liu, Z. P. Lu, J. Y. He, J. H. Luan, Z. J. Wang, B. Liu, Y. Liu, M. W. Chen, C. T. Liu, *Acta Mater.* **2016**, 116, 332.
- [10] S. Praveen, J. Basu, S. Kashyap, R. Kottada, *J. Alloys Compd.* **2016**, 662, 361.
- [11] J. Wang, T. Guo, J. Li, W. Jia, H. Kou, *Mater. Chem. Phys.* **2018**, 210, 192.
- [12] E. Colombini, M. Lassinantti Gualtieri, C. Mortalò, S. M. Deambrosis, P. Veronesi, *Mater. Lett.* **2022**, 323, 132571.
- [13] L. Ma, C. Li, Y. Jiang, L. Wang, F. Wang, T. Cao, Y. Xue, *J. Alloys Compd.* **2017**, 694, 61.
- [14] H. Zheng, Q. Xu, R. Chen, G. Qin, X. Li, Y. Su, J. Guo, H. Fu, *Intermetallics* **2020**, 119, 106723.
- [15] H. Besharatloo, J. M. Wheeler, *J. Mater. Res.* **2021**, 36, 2198.
- [16] E. D. Hintsala, U. Hangen, D. D. Stauffer, *JOM* **2018**, 70, 494.
- [17] Y. Tong, H. Zhang, H. Huang, L. Yang, Y. Hu, X. Liang, M. Hua, J. Zhang, *Intermetallics* **2021**, 135, 107209.
- [18] Y. Chen, E. Hintsala, N. Li, B. R. Becker, J. Y. Cheng, B. Nowakowski, J. Weaver, D. Stauffer, N. A. Mara, *JOM* **2019**, 71, 3368.
- [19] D. You, G. Yang, Y.-H. Choa, J. K. Kim, *Mater. Sci. Eng., A* **2022**, 831, 142039.
- [20] F. G. Coury, P. Wilson, K. D. Clarke, M. J. Kaufman, A. J. Clarke, *Acta Mater.* **2019**, 167, 1.
- [21] A. Hilhorst, P. J. Jacques, *J. Phase Equilib. Diffus.* **2021**, 42, 708.
- [22] D. Chung, Z. Ding, Y. Yang, *Adv. Eng. Mater.* **2019**, 21, 1801060.
- [23] S. Muskeri, D. Choudhuri, P. A. Jannotti, B. E. Schuster, J. T. Lloyd, R. S. Mishra, S. Mukherjee, *Adv. Eng. Mater.* **2020**, 22, 2000124.
- [24] W. D. Nix, H. Gao, *J. Mech. Phys. Solids* **1998**, 46, 411.
- [25] R. Rodrigues, I. Gutierrez, *Mater. Sci. Eng., A* **2003**, 361, 377.
- [26] G. M. Pharr, E. G. Herbert, Y. Gao, *Annu. Rev. Mater. Res.* **2010**, 40, 271.
- [27] K. Durst, B. Backes, O. Franke, M. Göken, *Acta Mater.* **2006**, 54, 2547.
- [28] K. Durst, B. Backes, M. Göken, *Scr. Mater.* **2005**, 52, 1093.
- [29] Z. Wang, H. Bei, E. P. George, G. M. Pharr, *Scr. Mater.* **2011**, 65, 469.
- [30] S. Pathak, D. Stojakovic, R. Doherty, S. R. Kalidindi, *J. Mater. Res.* **2009**, 24, 1142.
- [31] D. F. Bahr, D. E. Kramer, W. W. Gerberich, *Acta Mater.* **1998**, 46, 3605.
- [32] Y. Liu, A. H. W. Ngan, *Scr. Mater.* **2000**, 44, 237.
- [33] L. Yang, Y. Chen, J. Miller, W. J. Weber, H. Bei, Y. Zhang, *Mater. Sci. Eng., A* **2022**, 856, 143685.
- [34] E. Colombini, M. Lassinantti Gualtieri, C. Mortalò, S. M. Deambrosis, F. Montagner, V. Zin, E. Miorin, G. Valsecchi, M. Fabrizio, P. Veronesi, *Adv. Eng. Mater.* **2022**, 24, 2101518.
- [35] U. Dahborg, J. Cornide, M. Calvo-Dahlborg, T. C. Hansen, A. Fitch, Z. Leong, S. Chambreland, R. Goodall, *J. Alloys Compd.* **2016**, 681, 330.
- [36] K. Durst, M. Göken, H. Vehoff, *J. Mater. Res.* **2004**, 19, 85.
- [37] L. J. Zhang, M. D. Zhang, Z. Zhou, J. T. Fan, P. Cui, P. F. Yu, Q. Jing, M. Z. Ma, P. K. Liaw, G. Li, R. P. Liu, *Mater. Sci. Eng., A* **2018**, 725, 437.
- [38] J. Guo, M. Goh, Z. Zhu, X. Lee, M. L. S. Nai, J. Wei, *Mater. Des.* **2018**, 153, 211.
- [39] X. Li, B. Bhushan, *Mater. Charact.* **2002**, 48, 11.
- [40] A. Ruiz-Moreno, P. Hähner, *Mater. Des.* **2018**, 145, 168.
- [41] G. M. Pharr, J. H. Strader, W. C. Oliver, *J. Mater. Res.* **2009**, 24, 653.
- [42] P. Haušild, *Philos. Mag.* **2021**, 101, 420.
- [43] E. Broitman, *Tribol. Lett.* **2017**, 65, 23.
- [44] W. C. Oliver, G. M. Pharr, *J. Mater. Res.* **1992**, 6, 1564.
- [45] P. Sudharshan Phani, W. C. Oliver, *Mater. Des.* **2019**, 164, 107563.
- [46] G. Constantinides, K. S. Ravi Chandran, F.-J. Ulm, K. J. Van Vliet, *Mater. Sci. Eng., A* **2006**, 430, 189.